Available online at www.sciencedirect.com
ScienceDirect
Journal of Sound and Vibration 299 (2007) 484–503
JOURNAL OF SOUND AND VIBRATION
www.elsevier.com/locate/jsvi

Hybrid power flow analysis using coupling loss factor of SEA for low-damping system—Part I: Formulation of 1-D and 2-D cases

Young-Ho Park, Suk-Yoon Hong*

Department of Naval Architecture and Ocean Engineering, Seoul National University, San 56-1 Sillim-dong, Gwanak-gu, Seoul 151-742, Republic of Korea

Received 5 August 2004; received in revised form 25 January 2006; accepted 27 March 2006
Available online 2 October 2006

Abstract

This paper proposes a hybrid method for the prediction of vibrational and acoustic responses of low-damping system in the medium-to-high frequency ranges by using the power flow analysis (PFA) algorithm and statistical energy analysis (SEA) coupling concepts. The main part of this method is the application of the coupling loss factor (CLF) of SEA to the boundary condition of PFA in reverberant system. First, for hybrid PFA, the hybrid boundary conditions on 1-D and 2-D cases were derived in the general form. To verify the derived boundary conditions, numerical analyses for each case were performed. The hybrid PFA solutions using derived boundary conditions were compared with the classical PFA solutions with various reverberance factors including the effects of the characteristic length, excitation frequency and group velocity besides damping loss factor of the subsystem. Additionally, the hybrid PFA on 3-D case and the hybrid power flow finite element method (PFFEM) for hybrid PFA of built-up structures are described in the other companion paper.

1. Introduction

Much of the current vibration analyses of structure-borne noise have been done by using the traditional finite element method (FEM). However, as the excitation frequency increases, the vibrational wavelength in a structure decreases. To properly model high-frequency vibrations, either the order of shape functions in FEM must be increased or the size of mesh decreased. Therefore, finite element models are disadvantageous for performing accurate high-frequency analysis because they become too large for efficient application [1,2]. In addition, the traditional finite element method is essentially a deterministic analysis technique. The method requires all the data for a problem to be known exactly. At low frequencies, data such as material properties and joint behavior are reasonably well known and the solution is not highly sensitive to their typical variations. However, at high frequencies, the required data for structural dynamic problems is uncertain, and thus, the solution is highly sensitive to data variations. Therefore, at high frequencies, the statistical approach for analyzing structural and acoustic responses is more appropriate than the deterministic one.

*Corresponding author. Tel.: +82 2 880 8757; fax: +82 2 888 9298.
E-mail address: syh@snu.ac.kr (S.-Y. Hong).

0022-460X/$ - see front matter © 2006 Elsevier Ltd. All rights reserved.
doi:10.1016/j.jsv.2006.03.055

Statistical energy analysis (SEA) has become a widely accepted technique for modeling high-frequency, dynamic responses of vibro-acoustic systems of high modal density. In SEA, each component of a built-up system is treated as a statistical population of mode groups and the average dynamic response of component parts calculated [3]. Therefore, the analytic model for SEA is very simple compared with that for common FEA. However, because assumptions in the development of SEA are simplified, the analytic results are not sufficiently reliable in the low-to-medium frequency ranges. Additionally, SEA gives no information about the spatial distribution of dynamic responses such as energy, acceleration, etc. within a given subsystem.

General energy analysis (GEA) formulates the vibrational problem of structures in a purely energetic form without approximation [4]. Therefore, the results obtained by GEA are exact when compared to those obtained using the displacement solution to the vibrational wave equation. However, GEA is more computationally intensive than the classical exact solutions in 1-D vibrational problems and the development of general energy formulation and coupling relationship for higher-order structures such as plates has not been achieved yet.

Power flow analysis (PFA) is understood to be one of reliable methods, and has remarkable advantages compared to other analytic tools for the prediction of vibrational and acoustic responses in the medium-to-high frequency ranges. PFA models the flow of mechanical energy in a manner analogous to the flow of thermal energy in heat conduction. Because the governing equation for energy distribution in steady state condition is spatial differential equation, PFA gives information about the spatial variation of intensity as well as energy density. Additionally, power flow finite element method (PFFEM) that applies PFA to the finite element technique can present the consistent analytic result regardless of modelers.

Many researchers have developed SEA since 1959. SEA has much information, especially about the coupling data, which are important in the vibro-acoustic analysis of built-up structures and has some commercialized softwares/hardwares calculating SEA parameters such as coupling loss factor (CLF), modal density, damping loss factor, etc. This coupling information can be used efficiently in an alternative method based on energy. In particular, the commercialized NVH software based on energy must support the functions that simulate with the use of experimental parameters to increase the accuracy of analytic results. In this case, the coupling loss factor of SEA, which is easier to be obtained, can be used as very efficient information. In relation to these, Langley has shown a simple methodology which uses CLF in the boundary condition of PFA about one kind of motion in a 2-D structure for the different object [5].

In this paper, the general algorithm for the use of CLF in PFA boundary condition was presented. Formulation using CLF in PFA boundary condition was developed to cover the all kinds of propagating waves of one- and 2-D cases, and was proven to be valid through numerical analyses of each dimensional case. Additionally, the hybrid PFA for the 3-D case and the hybrid PFFEM to extend the application area of the developed hybrid method to built-up structures will be described in the other companion paper [6].

2. Formulation of hybrid boundary condition in power flow analysis

2.1. 1-D case

The equation of motion for the uniform Bernoulli–Euler beam excited by a transverse harmonic point force is

$$E_c I \frac{\partial^4 w}{\partial x^4} + \rho S \frac{\partial^2 w}{\partial t^2} = F\delta(x - x_0)\, e^{j\omega t}. \tag{2.1}$$

Here $E_c = E(1 + j\eta)$ is the complex modulus of elasticity, E is the Young's modulus, η is the hysteretic damping loss factor, I is the moment of inertia, ρ is the density, S is the sectional area, ω is the excitation frequency, w is the transverse displacement, and $F\delta(x - x_0)\, e^{j\omega t}$ is the harmonic point force applied at point x_0.

The general solution of Eq. (2.1) is

$$w(x, t) = \left(A_1 e^{-jk_c x} + A_2 e^{jk_c x} + A_3 e^{-k_c x} + A_4 e^{k_c x}\right) e^{j\omega t}, \tag{2.2}$$

where A_i is the complex coefficient and k_c is a complex wavenumber defined by the expression:

$$k_c = \left(\frac{\omega}{c_p}\right)\sqrt[4]{\frac{(1-\mathrm{j}\eta)}{(1+\eta^2)}}, \tag{2.3}$$

where $c_p = \sqrt[4]{\omega^2 EI/\rho S}$ is the phase velocity of the flexural wave in beam.

In lightly damped structures, that is, $\eta \ll 1$, the real and imaginary components of the complex wavenumber k_c, k_1 and k_2 are well approximated as, respectively [1]

$$k_1 = \omega/c_p, \quad k_2 = -(\eta/4)k_1. \tag{2.4}$$

Total power in the transversely vibrating beam may be separated into one that is associated with the shear force and the other with the bending moment. The time-averaged total flexural power can be represented as

$$\langle q\rangle_f = \frac{1}{2}\mathrm{Re}\left\{-V\frac{\partial w^*}{\partial t}\right\} + \frac{1}{2}\mathrm{Re}\left\{-M\frac{\partial^2 w^*}{\partial x \partial t}\right\}, \tag{2.5}$$

where $V = -E_c I\left(\partial^3 w/\partial x^3\right)$ is shear force, $M = E_c I\left(\partial^2 w/\partial x^2\right)$ is bending moment and the sign of asterisk means the complex conjugate.

The time-averaged total flexural energy density by transverse displacement (Eq. (2.2)) is the sum of its potential energy density and the kinetic energy density:

$$\langle e\rangle_f = \langle e\rangle_{\text{potential}} + \langle e\rangle_{\text{kinetic}} = \frac{1}{4}EI\left\{\frac{\partial^2 w}{\partial x^2}\frac{\partial^2 w^*}{\partial x^2}\right\} + \frac{1}{4}\rho S\left\{\frac{\partial w}{\partial t}\frac{\partial w^*}{\partial t}\right\}. \tag{2.6}$$

Goyder et al. [7] and Wohlever [8] have shown that the far-field component of energy and power is dominant at high frequencies. Therefore, the time-averaged far-field total flexural power in which near-field terms are neglected is represented as

$$\langle q\rangle_f = EI\omega k_1^3\left(|A_1|^2\,\mathrm{e}^{2k_2 x} - |A_2|^2\,\mathrm{e}^{-2k_2 x}\right) = \langle q\rangle_f^+ - \langle q\rangle_f^-, \tag{2.7}$$

where $\langle q\rangle_f^+$ and $\langle q\rangle_f^-$ mean the positive- and negative-directional flexural powers, respectively.

The time- and locally space-averaged far-field total flexural energy density in which spatially harmonic terms are eliminated is represented as

$$\langle e\rangle_f = \frac{1}{2}\rho S\omega^2\left(|A_1|^2\,\mathrm{e}^{2k_2 x} + |A_2|^2\,\mathrm{e}^{-2k_2 x}\right) = \langle e\rangle_f^+ + \langle e\rangle_f^-, \tag{2.8}$$

where $\langle e\rangle_f^+$ and $\langle e\rangle_f^-$ mean the positive- and negative-directional flexural energy densities, respectively.

Using Eqs. (2.7) and (2.8), the relationship between the time- and locally space-averaged flexural energy density and power can be represented as

$$\langle q\rangle_f = -\frac{c_{gf}^2}{\eta\omega}\frac{\mathrm{d}\langle e\rangle_f}{\mathrm{d}x} = \langle q\rangle_f^+ - \langle q\rangle_f^- = c_{gf}\langle e\rangle_f^+ - c_{gf}\langle e\rangle_f^-, \tag{2.9}$$

where $c_{gf} = 2\left(\omega^2 EI/\rho S\right)^{1/4}$ is the group velocity of flexural wave in the Bernoulli–Euler beam.

Using Eq. (2.9) and the energy balance equation in a steady state, the energy governing equation for flexural wave in the Bernoulli–Euler beam can be represented as

$$-\frac{c_{gf}^2}{\eta\omega}\frac{\mathrm{d}^2\langle e\rangle_f}{\mathrm{d}x^2} + \eta\omega\langle e\rangle_f = \Pi_{\mathrm{in},f}. \tag{2.10}$$

In case of longitudinal vibration in a beam, the relationship between time-averaged energy density and power like flexural vibration can be represented as [1]

$$\langle q\rangle_l = -\frac{c_{gl}^2}{\eta\omega}\frac{\mathrm{d}\langle e\rangle_l}{\mathrm{d}x} = \langle q\rangle_l^+ - \langle q\rangle_l^- = c_{gl}\langle e\rangle_l^+ - c_{gl}\langle e\rangle_l^-, \tag{2.11}$$

where $c_{gl} = \sqrt{E/\rho}$ is the group velocity for longitudinal wave in a beam. Using Eq. (2.11), the energy governing equation for longitudinal wave in a beam like that of flexural wave can be represented as

$$-\frac{c_{gl}^2}{\eta\omega}\frac{d^2\langle e\rangle_l}{dx^2} + \eta\omega\langle e\rangle_l = \Pi_{\mathrm{in},l}. \tag{2.12}$$

The general solution of Eqs. (2.10) and (2.12) can be expressed as the following form:

$$\langle e\rangle_m = B_1 \times \exp\left(-\psi_m x\right) + B_2 \times \exp\left(\psi_m x\right), \quad (m = f, l), \tag{2.13}$$

where B_i is the constant coefficient and $\psi_m = \eta\omega/c_{gm}$.

The time- and locally space-averaged energy density solution of m-type wave in Eq. (2.13) is composed of not propagating wave components but exponentially decaying wave components. Additionally, the value of ψ_m in Eq. (2.13) means the decay rate of m-type energy density per unit length. Therefore, the reverberance factor ($\Re_m = \psi_m L_c$) which represents how reverberant the wave-field (subsystem) is, can be defined by multiplying ψ_m by the characteristic length (L_c) of the subsystem and is related to the excitation frequency, group velocity and characteristic length besides damping loss factor of the subsystem. If the reverberance factor $\mathfrak{R}_{\mathrm{m}}$ of m-type wave-field in a subsystem is zero, the wave-field is completely reverberant ($\langle e\rangle_m = \text{constant}$). Generally, if the hysteretic damping of a structural subsystem is very small like common metal, the size of a subsystem is not very large, and the exciting frequency is not very high, energy density will vary little within the subsystem except for loaded subsystem. In this case, the assumption that the energy density in a subsystem is constant, that is, the wave-field is reverberant, will not be unreasonable.

If the energy density field of each beam in a coupled beam structure shown in Fig. 1 is assumed to be reverberant and the system contains a modal overlap, the power which is transferred from m-type waves in beam 1 to n-type waves in beam 2 can be expressed as

$$\Pi_{1m\to 2n} = \omega\eta_{12mn}E_{1m} = \omega\eta_{12mn}L_1\langle e\rangle_{1m}, \tag{2.14}$$

where E_{1m} is the total energy, $\langle e\rangle_{1m}$ is the energy density per unit length of an m-type wave, L_1 is the length of beam 1, and η_{12mn} is the coupling loss factor from m-type waves in beam 1 to n-type waves in beam 2. The coupling loss factor for point junction among beams in Eq. (2.14) is known as

$$\eta_{12mn} = \frac{c_{g1m}\langle\tau\rangle_{12mn}}{2\omega L_1}, \tag{2.15}$$

where $\langle\tau\rangle_{12mn}$ is the power transmission coefficient of n-type wave in beam 2 due to m-type wave in beam 1.

Using Eqs. (2.9) and (2.14), the net power of a flexural wave from beam 1 to beam 2 can be represented as

$$\Pi_{1f2m} = -\frac{c_{g1f}^2}{\eta_1\omega}\frac{\mathrm{d}\langle e_1\rangle_f}{\mathrm{d}x_1} = \sum_{m=f,l}\left(\Pi_{1f\to 2m} - \Pi_{2m\to 1f}\right) = \sum_{m=f,l}\left\{\omega\left(L_1\eta_{12fm}\langle e_1\rangle_f - L_2\eta_{21mf}\langle e_2\rangle_m\right)\right\}, \tag{2.16}$$

and

$$\Pi_{1m2f} = -\frac{c_{g2f}^2}{\eta_2\omega}\frac{\mathrm{d}\langle e_2\rangle_f}{\mathrm{d}x_2} = \sum_{m=f,l}\left(\Pi_{1m\to 2f} - \Pi_{2f\to 1m}\right) = \sum_{m=f,l}\left\{\omega\left(L_1\eta_{12mf}\langle e_1\rangle_m - L_2\eta_{21fm}\langle e_2\rangle_f\right)\right\}. \tag{2.17}$$

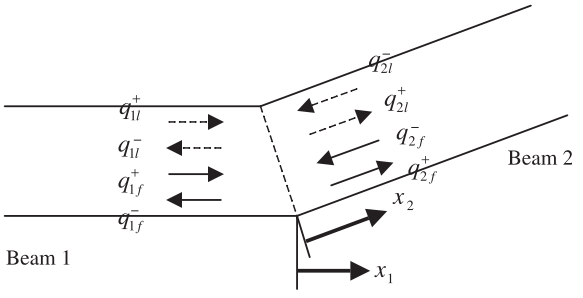

Fig. 1. Power flow model of two semi-infinite beams joined at an arbitrary angle.

For a longitudinal wave, the net power from beam 1 to beam 2 using Eqs. (2.11) and (2.14) can be represented as

$$\Pi_{1l2m} = -\frac{c_{g1l}^2}{\eta_1\omega}\frac{\mathrm{d}\langle e_1\rangle_l}{\mathrm{d}x_1} = \sum_{m=f,l}(\Pi_{1l\to 2m} - \Pi_{2m\to 1l}) = \sum_{m=f,l}\left\{\omega\left(L_1\eta_{12lm}\langle e_1\rangle_l - L_2\eta_{21ml}\langle e_2\rangle_m\right)\right\}, \tag{2.18}$$

and

$$\Pi_{1m2l} = -\frac{c_{g2l}^2}{\eta_2\omega}\frac{\mathrm{d}\langle e_2\rangle_l}{\mathrm{d}x_2} = \sum_{m=f,l}(\Pi_{1m\to 2l} - \Pi_{2l\to 1m}) = \sum_{m=f,l}\left\{\omega\left(L_1\eta_{12ml}\langle e_1\rangle_m - L_2\eta_{21lm}\langle e_2\rangle_l\right)\right\}. \tag{2.19}$$

The upper equations (2.16)–(2.19) represent the hybrid boundary condition in local coordinate mixing the concepts of PFA and SEA, using the power transfer relation in reverberant field. That is, using the advantages of each method, the power flow solution such as Eq. (2.13) is used within the domain and the coupling relationship of SEA such as Eq. (2.14) is used in the boundary. If N beams are joined at arbitrary angles as shown in Fig. 2, $2N$ boundary conditions at the point junction are required for power flow analysis and can be represented as

$$-\frac{c_{gif}^2}{\eta_i\omega}\frac{\mathrm{d}\langle e_i\rangle_f}{\mathrm{d}x_i} = \sum_{j=1,j\neq i}^{N}\left[\sum_{m=f,l}\left\{\omega\left(L_i\eta_{ijfm}\langle e_i\rangle_f - L_j\eta_{jimf}\langle e_j\rangle_m\right)\right\}\right] \quad (i=1,\ldots,N), \tag{2.20}$$

and

$$-\frac{c_{gil}^2}{\eta_i\omega}\frac{\mathrm{d}\langle e_i\rangle_l}{\mathrm{d}x_i} = \sum_{j=1,j\neq i}^{N}\left[\sum_{m=f,l}\left\{\omega\left(L_i\eta_{ijlm}\langle e_i\rangle_l - L_j\eta_{jiml}\langle e_j\rangle_m\right)\right\}\right] \quad (i=1,\ldots,N), \tag{2.21}$$

where $-(c_{gif}^2/\eta_i\omega)(\mathrm{d}\langle e_i\rangle_f/\mathrm{d}x_i)$ and $-(c_{gil}^2/\eta_i\omega)(\mathrm{d}\langle e_i\rangle_l/\mathrm{d}x_i)$ are net flexural and longitudinal powers in beam i, respectively, $\langle e_i\rangle_m$ is m-type energy density of beam i, and η_{ijmn} is coupling loss factor form m-type waves in beam i to n-type waves in beam j. If the beam structure is not composed of co-planer beams, the terms of torsional energy density and power have to be added in Eqs. (2.20) and (2.21) for hybrid power flow analysis.

However, if the hysteretic damping of a structural subsystem is not small, the size of a subsystem is very large, or the exciting frequency is very high, the energy density in its subsystem will vary greatly and its field

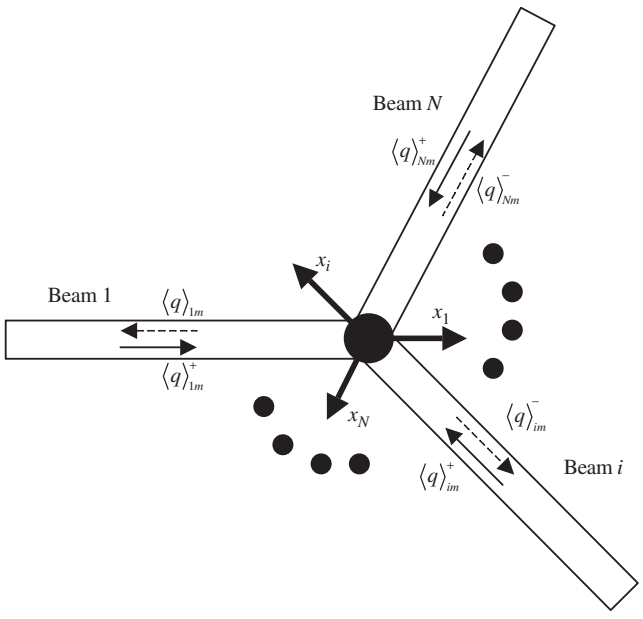

Fig. 2. General hybrid power flow model of N beams joined at arbitrary angles.

will be not reverberant any more due to large reverberance factor. In this case, the values of energy density and power in the boundary cannot represent those spatially averaged in the subsystem. Therefore, the hybrid boundary condition at the joint of highly damped structures may generate more error than the classical boundary condition. In case of two coupled co-planer beams, the classical boundary condition in PFA using the power transmission and reflection coefficients derived by wave transmission approach is expressed as

$$\langle q\rangle_{2f}^{+} = \langle \tau_{12ff}\rangle\langle q\rangle_{1f}^{+} + \langle \gamma_{22ff}\rangle\langle q\rangle_{2f}^{-} + \langle \tau_{12lf}\rangle\langle q\rangle_{1l}^{+} + \langle \gamma_{22lf}\rangle\langle q\rangle_{2l}^{-}, \tag{2.22a}$$

$$\langle q\rangle_{1f}^{-} = \langle \gamma_{11ff}\rangle\langle q\rangle_{1f}^{+} + \langle \tau_{21ff}\rangle\langle q\rangle_{2f}^{-} + \langle \gamma_{11lf}\rangle\langle q\rangle_{1l}^{+} + \langle \tau_{21lf}\rangle\langle q\rangle_{2l}^{-}, \tag{2.22b}$$

$$\langle q\rangle_{2l}^{+} = \langle \tau_{12fl}\rangle\langle q\rangle_{1f}^{+} + \langle \gamma_{22fl}\rangle\langle q\rangle_{2f}^{-} + \langle \tau_{12ll}\rangle\langle q\rangle_{1l}^{+} + \langle \gamma_{22ll}\rangle\langle q\rangle_{2l}^{-}, \tag{2.22c}$$

and

$$\langle q\rangle_{1l}^{-} = \langle \gamma_{11fl}\rangle\langle q\rangle_{1f}^{+} + \langle \tau_{21fl}\rangle\langle q\rangle_{2f}^{-} + \langle \gamma_{11ll}\rangle\langle q\rangle_{1l}^{+} + \langle \tau_{21ll}\rangle\langle q\rangle_{2l}^{-}, \tag{2.22d}$$

where $\langle q\rangle_{f}^{+}$ and $\langle q\rangle_{l}^{+}$ are the flexural and longitudinal components of power in the positive direction, respectively, $\langle \gamma_{iimn}\rangle$ is the power reflection coefficient of n-type wave in beam i due to m-type wave in beam i, and all the powers are the values in the boundary.

Since the sum of the power transmission and reflection coefficients is one, the sum of Eqs. (2.22a)–(2.22d)

$$\langle q\rangle_{1f}^{+} - \langle q\rangle_{1f}^{-} + \langle q\rangle_{1l}^{+} - \langle q\rangle_{1l}^{-} = \langle q\rangle_{2f}^{+} - \langle q\rangle_{2f}^{-} + \langle q\rangle_{2l}^{+} - \langle q\rangle_{2l}^{-}. \tag{2.23}$$

Based on the relation of energy density and power, Eq. (2.23) can be expressed as

$$-\frac{c_{g1f}^2}{\eta_1\omega}\frac{\mathrm{d}\langle e_1\rangle_f}{\mathrm{d}x_1} - \frac{c_{g1l}^2}{\eta_1\omega}\frac{\mathrm{d}\langle e_1\rangle_l}{\mathrm{d}x_1} = -\frac{c_{g2f}^2}{\eta_2\omega}\frac{\mathrm{d}\langle e_2\rangle_f}{\mathrm{d}x_2} - \frac{c_{g2l}^2}{\eta_2\omega}\frac{\mathrm{d}\langle e_2\rangle_l}{\mathrm{d}x_2}. \tag{2.24}$$

Eq. (2.24) can be also obtained summing Eqs. (2.16)–(2.19) that are hybrid boundary conditions.

2.1.1. Numerical examples

To verify the usefulness of the new hybrid boundary condition on 1-D case, this condition was numerically applied to three finite beams joined at arbitrary angles as shown in Fig. 3. To consider an arbitrary case, the dimensions ($L \times B \times H$) of beams were assumed to be $2\,\mathrm{m} \times 0.01\,\mathrm{m} \times 0.01\,\mathrm{m}$, $2\,\mathrm{m} \times 0.03\,\mathrm{m} \times 0.03\,\mathrm{m}$ and $2\,\mathrm{m} \times 0.03\,\mathrm{m} \times 0.03\,\mathrm{m}$, respectively. Beams 1 and 2 were made of steel ($E_{1,2} = 19.5 \times 10^{10}\,\mathrm{Pa}$, $\rho_{1,2} = 7800\,\mathrm{kg/m^3}$) and beam 3 of aluminum ($E_3 = 7.1 \times 10^{10}\,\mathrm{Pa}$, $\rho_3 = 2700\,\mathrm{kg/m^3}$). The angle θ_1, between beams 1 and 2 was assumed to be 45° and θ_2 between beams 2 and 3 to be −45°. The magnitude of the flexural point force applied in the center of incident beam is 100 N. The time-averaged input power can be

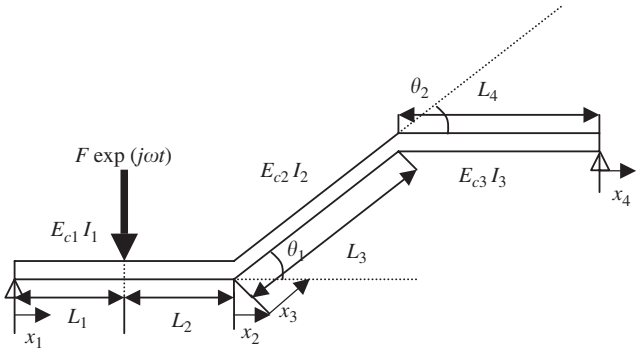

Fig. 3. Three finite beams jointed at arbitrary angles.

calculated as follows:

$$\Pi_{\text{in}} = \frac{1}{2}\text{Re}\left\{ \left(F e^{j\omega t}\right) \times \left(\frac{\partial w(x_0)}{\partial t}\right)^{*} \right\}, \tag{2.25}$$

where $w(x_0)$ is the transverse displacement at the loading point. For the first model, the structural damping values of all beams were assumed to be $\eta = 0.1$. For the second model, to consider the effect of reverberance factor, the structural damping values of all beams were changed into $\eta = 0.01$ corresponding to the value of common metals. The detailed procedure of numerical analysis for 1-D case is discussed in Appendix A.1.

Figs. 4–7 show the numerical results obtained using each boundary condition in all joints of the first model for 1/3 octave band with $f_c = 5\,\text{kHz}$ and $\eta = 0.1$. In this model, the reverberance factors of flexural and longitudinal wave-fields in each beam are $\Re_{f1} = 4.67$, $\Re_{f2} = 2.69$, $\Re_{f3} = 2.67$, $\Re_{l1} = 1.26$, $\Re_{l2} = 1.26$ and $\Re_{l3} = 1.23$, respectively. As expected, the flexural energy density of classical exact solution decreases universally with increasing distance from the excitation location and fluctuates locally in space, especially near the ends of beams and the junction in Fig. 4. The flexural energy density of power flow solutions, which is obtained using the hybrid and classical boundary conditions at the joints, varies smoothly in space without any fluctuation and has a discontinuity line at the junction. The classical exact solutions fluctuate in the vicinity of smoothed results of the power flow solutions obtained using hybrid and classical boundary conditions. The results of power flow solutions, which are obtained using hybrid and classical boundary conditions, generally agree with those of the classical exact solutions. However, because of large reverberance factors ($\Re_f \gg 0$), the flexural wave-field is not reverberant any more, and the values of energy density and power in the boundary are not equivalent to those of space-averaged energy density and power. Therefore, the difference between results obtained using hybrid and classical boundary conditions widens as the distance from excitation position increases. This phenomenon also appears in the results of longitudinal energy (Fig. 5), flexural power (Fig. 6) and longitudinal power (Fig. 7) besides the flexural energy (Fig. 4). In addition, because the reverberance factors of flexural wave-field are more than twice as large as those of longitudinal wave-field, the spatial variation of quantities of flexural wave-field in the subsystem is wider than that of quantities of longitudinal wave-field.

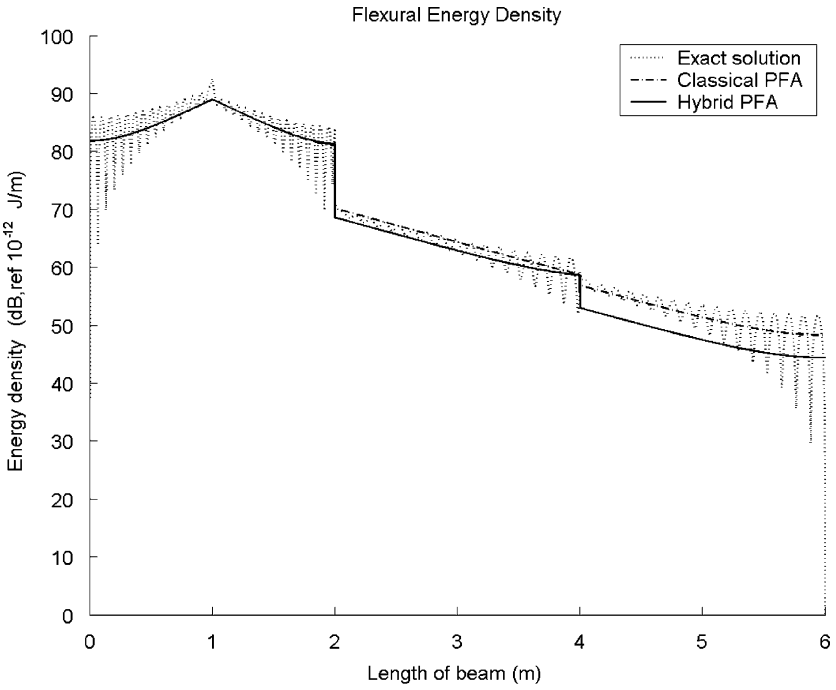

Fig. 4. Flexural energy density distribution of first model in $f = 5\,\text{kHz}$ and $\eta = 0.1$ ($\Re_{f1} = 4.67$, $\Re_{f2} = 2.69$, $\Re_{f3} = 2.67$). ——, hybrid PFA solution; - - - -, classical PFA solution; ⋯⋯, exact solution.

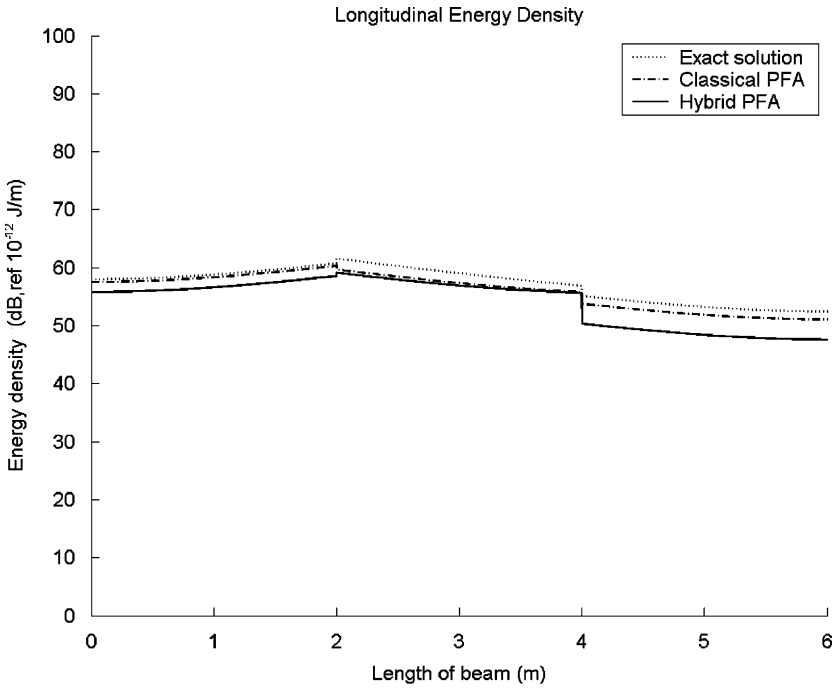

Fig. 5. Longitudinal energy density distribution of first model in $f = 5$ kHz and $\eta = 0.1$ ($\Re_{l1} = 1.26$, $\Re_{l2} = 1.26$, $\Re_{l3} = 1.23$). ——, hybrid PFA solution; - - - - -, classical PFA solution; ……, exact solution.

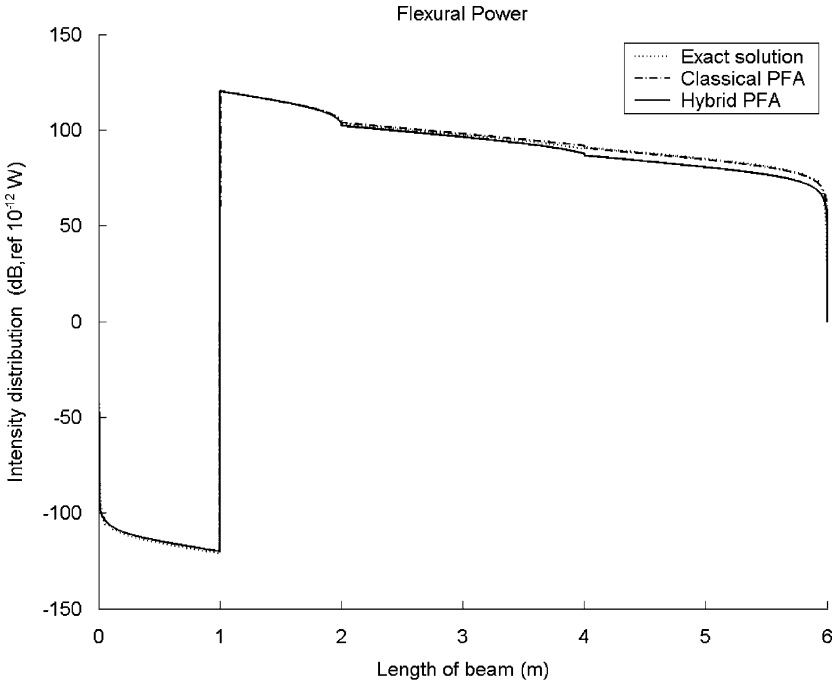

Fig. 6. Flexural power distribution of first model in $f = 5$ kHz and $\eta = 0.1$ ($\Re_{f1} = 4.67$, $\Re_{f2} = 2.69$, $\Re_{f3} = 2.67$). ——, hybrid PFA solution; - - - - -, classical PFA solution; ……, exact solution.

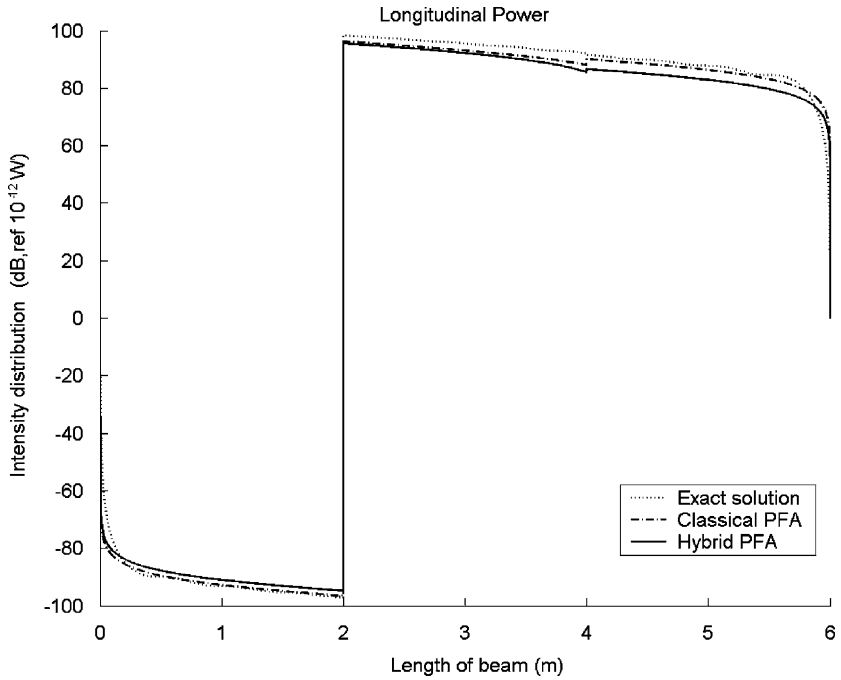

Fig. 7. Longitudinal power distribution of first model in $f = 5\,\text{kHz}$ and $\eta = 0.1$ ($\Re_{l1} = 1.26$, $\Re_{l2} = 1.26$, $\Re_{l3} = 1.23$). ——, hybrid PFA solution; - · - · -, classical PFA solution; ·····, exact solution.

Figs. 8 and 9 show the numerical results of classical power flow solutions, hybrid power flow solutions, and SEA solutions, which were obtained using each boundary condition in all joints for 1/3 octave band with $f_c = 5\,\text{kHz}$ and $\eta = 0.001$ The reverberance factors of each wave-field in the second model are one hundred times as small as those in the first model. Because the hybrid boundary condition is equivalent to the classical boundary condition when $\eta = 0$ ($\Re = 0$), the power flow solutions obtained using the hybrid boundary condition become equal to those obtained using the classical boundary condition, as the damping loss factor decreases. Therefore, Figs. 8 and 9 show that the results obtained using two boundary conditions agree well due to small reverberance factors. For the in-depth verification of hybrid boundary condition, Figs. 10 and 11 show the effect of reverberance factor in energy densities obtained using each boundary condition about flexural and longitudinal waves, respectively. In Figs. 10 and 11, the power flow solutions obtained using hybrid boundary condition were compared with those obtained using classical boundary condition at all joints. The relative difference in results shown in Figs. 10 and 11 is the value of the difference between space-averaged energy densities obtained using hybrid boundary condition and classical boundary condition, divided by the space-averaged energy density using classical boundary condition ($\|\overline{E_{3,\text{classic}}} - \overline{E_{3,\text{hybrid}}}\| / \|\overline{E_{3,\text{classic}}}\|$) in beam 3. As expected, the relative differences of flexural and longitudinal energy densities obtained using two boundary conditions approach zero as the reverberance factor of each beam decreases. Therefore, if the reverberance factor of wave-field in the beam is small, the power flow analysis using hybrid boundary condition will be effective.

2.2. 2-D case

The hybrid power flow analysis for 2-D case will be considered by expanding the algorithm in 1-D case. As an example of 2-D case, the energy governing equations of flexural, longitudinal, and shear waves in a homogeneous thin plate are represented as, respectively, [2,9]

$$-\frac{c_{gm}^2}{\eta\omega}\nabla^2\langle e\rangle_m + \eta\omega\langle e\rangle_m = \Pi_{\text{in},m} \quad (m = f, l, s), \tag{2.26}$$

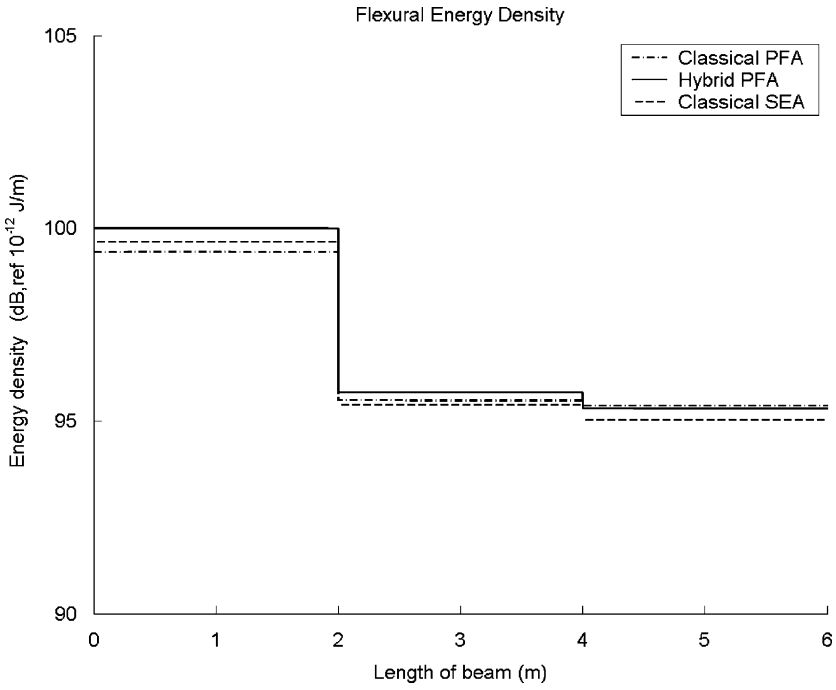

Fig. 8. Flexural energy density distribution of first model in $f = 5\,\text{kHz}$ and $\eta = 0.001$ ($\Re_{f1} = 0.0467$, $\Re_{f2} = 0.0269$, $\Re_{f3} = 0.0267$). ——, hybrid PFA solution; - · - · -, classical PFA solution; - - - - , classical SEA solution.

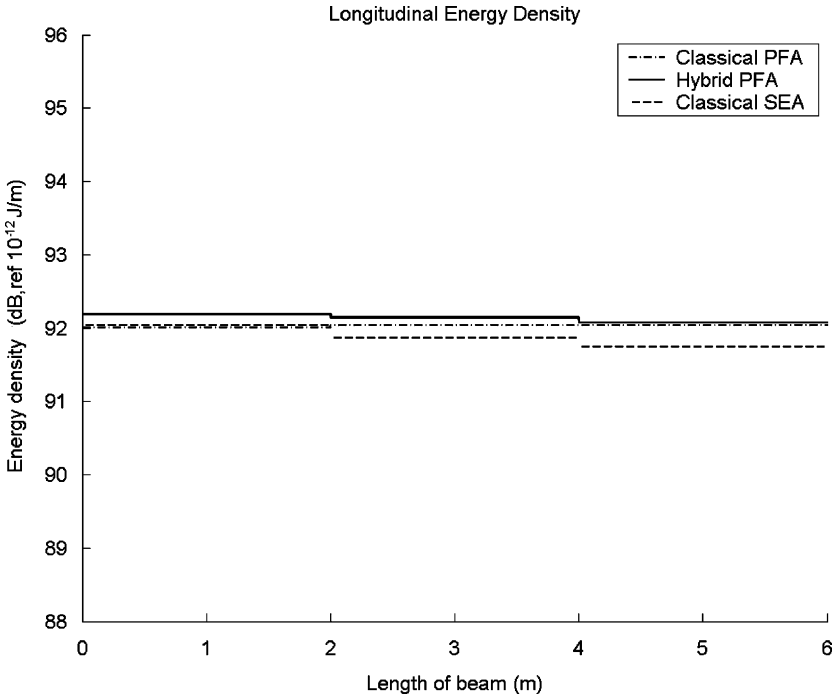

Fig. 9. Longitudinal energy density distribution of first model in $f = 5\,\text{kHz}$ and $\eta = 0.001$ ($\Re_{l1} = 0.0126$, $\Re_{l2} = 0.0126$, $\Re_{l3} = 0.0123$). ——, hybrid PFA solution; - · - · -, classical PFA solution; - - - - , classical SEA solution.

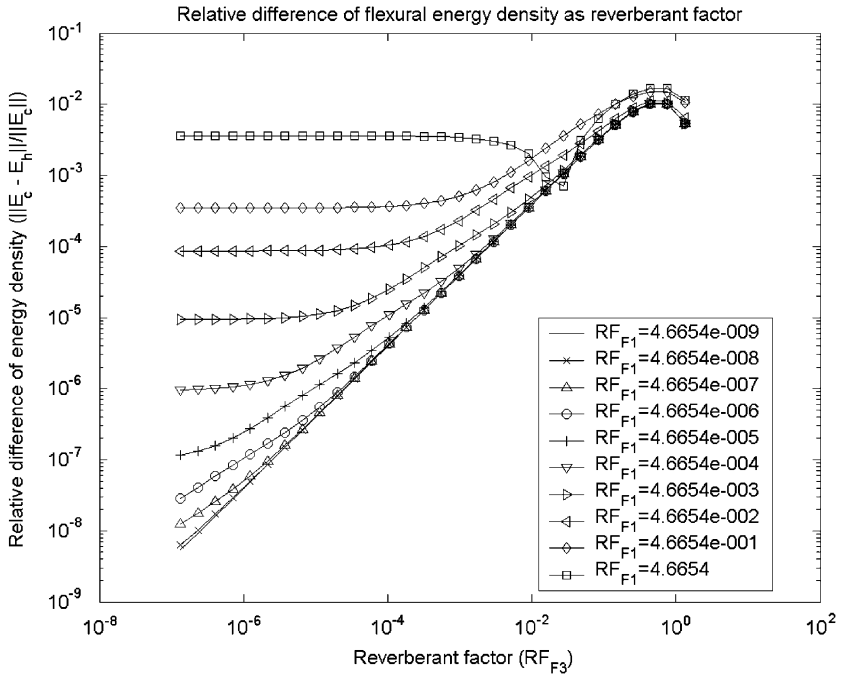

Fig. 10. Relative difference $\left(\|\overline{E_c}-\overline{E_h}\|/\|\overline{E_c}\|\right)$ of space-averaged flexural energy density by two methods in beam 3 as the reverberance factor variations of beam 1 and beam 3 in $f=5\,\text{kHz}$. ——, $\Re_{f1}=4.67\times10^{-9}$; —✕—, $\Re_{f1}=4.67\times10^{-8}$; —△—, $\Re_{f1}=4.67\times10^{-7}$; —○—, $\Re_{f1}=4.67\times10^{-6}$; —+—, $\Re_{f1}=4.67\times10^{-5}$; —▽—, $\Re_{f1}=4.67\times10^{-4}$; —▷—, $\Re_{f1}=4.67\times10^{-3}$; —◁—, $\Re_{f1}=4.67\times10^{-2}$; —◇—, $\Re_{f1}=4.67\times10^{-1}$; —□—, $\Re_{f1}=4.67$.

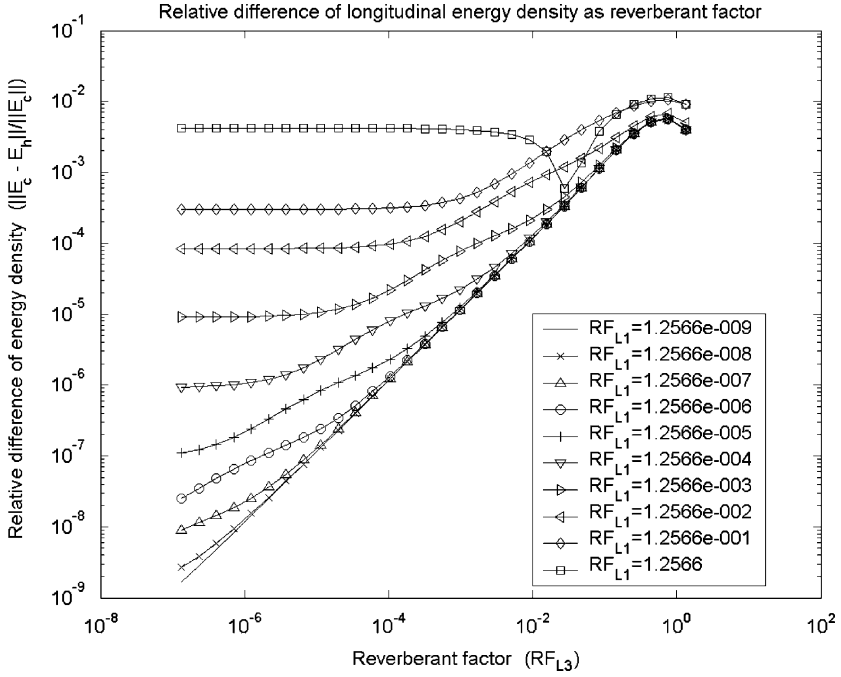

Fig. 11. Relative difference $\left(\|\overline{E_c}-\overline{E_h}\|/\|\overline{E_c}\|\right)$ of space-averaged longitudinal energy density by two methods in beam 3 as the reverberance factor variations of beams 1 and 3 in $f=5\,\text{kHz}$. ——, $\Re_{l1}=1.26\times10^{-9}$; —✕—, $\Re_{l1}=1.26\times10^{-8}$; —△—, $\Re_{l1}=1.26\times10^{-7}$; —○—, $\Re_{l1}=1.26\times10^{-6}$; —+—, $\Re_{l1}=1.26\times10^{-5}$; —▽—, $\Re_{l1}=1.26\times10^{-4}$; —▷—, $\Re_{l1}=1.26\times10^{-3}$; —◁—, $\Re_{l1}=1.26\times10^{-2}$; —◇—, $\Re_{l1}=1.26\times10^{-1}$; —□—, $\Re_{l1}=1.26$.

where c_{gm} is the group velocity of m-type wave and $\langle e\rangle_m$ are the time- and locally space-averaged far-field m-type energy densities, $\Pi_{in,m}$ is the input power of m-type wave component in a thin plate, and ∇^2 means Laplace operator.

For each wave in the plate, the relationship of the time- and locally space-averaged far-field energy density and intensity can be represented as [2,9]

$$\langle \vec{q}\rangle_m = -\frac{c_{gm}^2}{\eta\omega}\left(\frac{\partial}{\partial x}\vec{i}+\frac{\partial}{\partial y}\vec{j}\right)\langle e\rangle_m, \tag{2.27}$$

where $\langle \vec{q}\rangle_m$ is the time- and locally space-averaged far-field intensity of m-type wave.

Like the 1-D case, the reverberance factor $\Re_{\mathrm{m}}$ of m-type wave-field in a plate can be defined by

$$\Re_m = \psi_m L_c, \tag{2.28}$$

where L_c is the characteristic length of plate subsystem and $\psi_m = \eta\omega/c_{gm}$. If the reverberance factor of a wave-field in a subsystem is very small, the energy density field in the subsystem will be almost reverberant. In this case, because field values in the boundary can represent space-averaged field values of one subsystem, the hybrid boundary condition for plate structures can be derived. In the reverberant field, the power per unit length of line junction, which is transferred from m-type energy field in plate 1 to n-type energy field in plate 2, can be expressed by Eq. (2.29), using the coupling loss factor of SEA,

$$\Pi_{1m\to 2n} = \frac{\omega\eta_{12mn}E_{1,m}}{L} = \frac{\omega\eta_{12mn}S_1\langle e_1\rangle_m}{L}, \tag{2.29}$$

where $E_{1,m}$ is the total energy of m-type wave in plate 1, S_1 is the area of plate 1, η_{12mn} is the coupling loss factor from m-type wave in plate 1 to n-type wave in plate 2, L is the length of the line junction, and $\langle e_1\rangle_m$ is the energy density of the m-type wave in plate 1. In Eq. (2.29), the coupling loss factor for line junction among plates is known as

$$\eta_{12mn} = \frac{c_{g1m}\cdot L\cdot\langle\tau\rangle_{12mn}}{\omega\pi S_1}, \tag{2.30}$$

where c_{g1m} is the group velocity of m-type wave in plate 1.

Using Eqs. (2.27) and (2.29), the net power of flexural wave from plates 1 to 2 is represented as

$$\Pi_{1f2m} = -\frac{c_{g1f}^2}{\eta_1\omega}\nabla\langle e_1\rangle_f\cdot\vec{n} = \sum_{m=f,l,s}\left(\Pi_{1f\to 2m}-\Pi_{2m\to 1f}\right) = \sum_{m=f,l,s}\left\{\frac{\omega}{L}\left(S_1\eta_{12fm}\langle e_1\rangle_f - S_2\eta_{21mf}\langle e_2\rangle_m\right)\right\}, \tag{2.31}$$

and

$$\Pi_{1m2f} = -\frac{c_{g2f}^2}{\eta_2\omega}\nabla\langle e_2\rangle_f\cdot\vec{n} = \sum_{m=f,l,s}\left(\Pi_{1m\to 2f}-\Pi_{2f\to 1m}\right) = \sum_{m=f,l,s}\left\{\frac{\omega}{L}\left(S_1\eta_{12mf}\langle e_1\rangle_m - S_2\eta_{21fm}\langle e_2\rangle_f\right)\right\}, \tag{2.32}$$

where $\vec{n}$ is the normal vector shown in Fig. 12.

For a longitudinal wave, the net power from plates 1 to 2 can be represented as

$$\Pi_{1l2m} = -\frac{c_{g1l}^2}{\eta_1\omega}\nabla\langle e_1\rangle_l\cdot\vec{n} = \sum_{m=f,l,s}\left(\Pi_{1l\to 2m}-\Pi_{2m\to 1l}\right) = \sum_{m=f,l,s}\left\{\frac{\omega}{L}\left(S_1\eta_{12lm}\langle e_1\rangle_l - S_2\eta_{21ml}\langle e_2\rangle_m\right)\right\}, \tag{2.33}$$

and

$$\Pi_{1m2l} = -\frac{c_{g2l}^2}{\eta_2\omega}\nabla\langle e_2\rangle_l\cdot\vec{n} = \sum_{m=f,l,s}\left(\Pi_{1m\to 2l}-\Pi_{2l\to 1m}\right) = \sum_{m=f,l,s}\left\{\frac{\omega}{L}\left(S_1\eta_{12ml}\langle e_1\rangle_m - S_2\eta_{21lm}\langle e_2\rangle_l\right)\right\}. \tag{2.34}$$

For a shear wave, the net power from plates 1 to 2 can be also represented as

$$\Pi_{1s2m} = -\frac{c_{g1s}^2}{\eta_1\omega}\nabla\langle e_1\rangle_s\cdot\vec{n} = \sum_{m=f,l,s}\left(\Pi_{1s\to 2m}-\Pi_{2m\to 1s}\right) = \sum_{m=f,l,s}\left\{\frac{\omega}{L}\left(S_1\eta_{12sm}\langle e_1\rangle_s - S_2\eta_{21ms}\langle e_2\rangle_m\right)\right\}, \tag{2.35}$$

and

$$\Pi_{1m2s} = -\frac{c_{g2s}^2}{\eta_2 \omega} \nabla \langle e_2 \rangle_s \cdot \vec{n} = \sum_{m=f,l,s} (\Pi_{1m\to 2s} - \Pi_{2s\to 1m}) = \sum_{m=f,l,s} \left\{ \frac{\omega}{L} \left(S_1 \eta_{12ms} \langle e_1 \rangle_m - S_2 \eta_{21sm} \langle e_2 \rangle_s \right) \right\}. \quad (2.36)$$

The upper equations (2.31)–(2.36) represent the hybrid boundary condition of 2-D case in local coordinate mixing the concepts of PFA and SEA. To extend this boundary condition to the general form in 2-D case, if N plates are joined at arbitrary angles as shown in Fig. 13, $3N$ boundary conditions at the line junction are required for power flow analysis and can be derived as

$$-\frac{c_{gif}^2}{\eta_i \omega} \nabla \langle e_i \rangle_f \cdot \vec{n}_i = \sum_{j=1, j\neq i}^{N} \left[\sum_{m=f,l,s} \left\{ \frac{\omega}{L} \left(S_i \eta_{ijfm} \langle e_i \rangle_f - S_j \eta_{jimf} \left\langle e_j \right\rangle_m \right) \right\} \right] \quad (i = 1, \ldots, N), \quad (2.37)$$

$$-\frac{c_{gil}^2}{\eta_i \omega} \nabla \langle e_i \rangle_l \cdot \vec{n}_i = \sum_{j=1, j\neq i}^{N} \left[\sum_{m=f,l,s} \left\{ \frac{\omega}{L} \left(S_i \eta_{ijlm} \langle e_i \rangle_l - S_j \eta_{jiml} \left\langle e_j \right\rangle_m \right) \right\} \right] \quad (i = 1, \ldots, N), \quad (2.38)$$

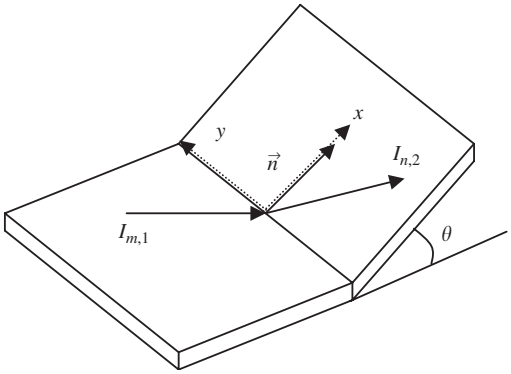

Fig. 12. Power flow model of two plates at arbitrary angle.

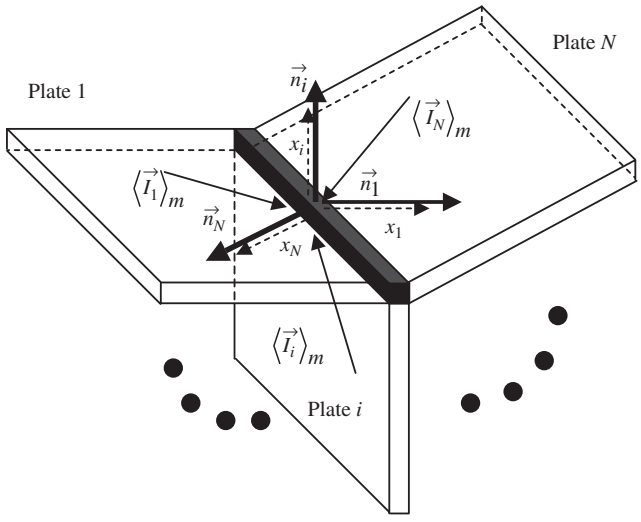

Fig. 13. General hybrid power flow model of N plates joined at arbitrary angles.

and

$$-\frac{c_{gis}^2}{\eta_i\omega}\nabla\langle e_i\rangle_s\cdot\vec{n}_i=\sum_{j=1,j\neq i}^{N}\left[\sum_{m=f,l,s}\left\{\frac{\omega}{L}\left(S_i\eta_{ijlm}\langle e_i\rangle_s-S_j\eta_{jims}\langle e_j\rangle_m\right)\right\}\right]\quad(i=1,\ldots,N),\tag{2.39}$$

where $-\left(c_{gim}^2\Big/\eta_i\omega\right)\nabla\langle e_i\rangle_m\cdot\vec{n}_i$ is net m-type power in plate i, $\langle e_i\rangle_m$ is m-type energy density of plate i, η_{ijmn} is coupling loss factor form m-type waves in plate i to n-type waves in plate j, and $\vec{n}_i$ is the normal vector of line junction in plate i.

In the classical power flow analysis, the boundary condition using diffuse power transmission and reflection coefficients, and intensity values in the joint of the model shown in Fig. 12 can be expressed as

$$\langle q_{1x}\rangle_f^-=\langle\gamma_{11ff}\rangle\langle q_{1x}\rangle_f^+ +\langle\gamma_{11lf}\rangle\langle q_{1x}\rangle_l^+ +\langle\gamma_{11sf}\rangle\langle q_{1x}\rangle_s^+ +\langle\tau_{21ff}\rangle\langle q_{2x}\rangle_f^- +\langle\tau_{21lf}\rangle\langle q_{2x}\rangle_l^- +\langle\tau_{21sf}\rangle\langle q_{2x}\rangle_s^-,$$

$$\langle q_{1x}\rangle_l^-=\langle\gamma_{11fl}\rangle\langle q_{1x}\rangle_f^+ +\langle\gamma_{11ll}\rangle\langle q_{1x}\rangle_l^+ +\langle\gamma_{11sl}\rangle\langle q_{1x}\rangle_s^+ +\langle\tau_{21fl}\rangle\langle q_{2x}\rangle_f^- +\langle\tau_{21ll}\rangle\langle q_{2x}\rangle_l^- +\langle\tau_{21sl}\rangle\langle q_{2x}\rangle_s^-,$$

$$\langle q_{1x}\rangle_s^-=\langle\gamma_{11fs}\rangle\langle q_{1x}\rangle_f^+ +\langle\gamma_{11ls}\rangle\langle q_{1x}\rangle_l^+ +\langle\gamma_{11ss}\rangle\langle q_{1x}\rangle_s^+ +\langle\tau_{21fs}\rangle\langle q_{2x}\rangle_f^- +\langle\tau_{21ls}\rangle\langle q_{2x}\rangle_l^- +\langle\tau_{21ss}\rangle\langle q_{2x}\rangle_s^-,$$

$$\langle q_{2x}\rangle_f^+=\langle\tau_{12ff}\rangle\langle q_{1x}\rangle_f^+ +\langle\tau_{12lf}\rangle\langle q_{1x}\rangle_l^+ +\langle\tau_{12sf}\rangle\langle q_{1x}\rangle_s^+ +\langle\gamma_{22ff}\rangle\langle q_{2x}\rangle_f^- +\langle\gamma_{22lf}\rangle\langle q_{2x}\rangle_l^- +\langle\gamma_{22sf}\rangle\langle q_{2x}\rangle_s^-,$$

$$\langle q_{2x}\rangle_l^+=\langle\tau_{12fl}\rangle\langle q_{1x}\rangle_f^+ +\langle\tau_{12ll}\rangle\langle q_{1x}\rangle_l^+ +\langle\tau_{12sl}\rangle\langle q_{1x}\rangle_s^+ +\langle\gamma_{22fl}\rangle\langle q_{2x}\rangle_f^- +\langle\gamma_{22ll}\rangle\langle q_{2x}\rangle_l^- +\langle\gamma_{22sl}\rangle\langle q_{2x}\rangle_s^-,$$

and

$$\langle q_{2x}\rangle_s^+=\langle\tau_{12fs}\rangle\langle q_{1x}\rangle_f^+ +\langle\tau_{12ls}\rangle\langle q_{1x}\rangle_l^+ +\langle\tau_{12ss}\rangle\langle q_{1x}\rangle_s^+ +\langle\gamma_{22fs}\rangle\langle q_{2x}\rangle_f^- +\langle\gamma_{22ls}\rangle\langle q_{2x}\rangle_l^- +\langle\gamma_{22ss}\rangle\langle q_{2x}\rangle_s^-\tag{2.40a–f}$$

2.2.1. Numerical examples

Numerical applications of hybrid power flow analysis for 2-D case are performed for three finite rectangular isotropic plates coupled at arbitrary angles and excited by a transverse harmonic point force, as shown in Fig. 14. The dimensions and thickness of the coupled plate structure shown in Fig. 14 are $L_{x1}=L_{x2}=L_{x3}=L_y=2\,\text{m}$ and $h=1\,\text{mm}$, respectively, and the material properties of the coupled plate structure are assumed to be the same as those of aluminum ($E=7.1\times10^{10}\,\text{Pa}$, $\rho=2700\,\text{kg/m}^3$). The transverse force is located at $x_0=L_{x1}/2$ and $y_0=L_y/2$ in plate 1 and its amplitude is $F=10\,\text{N}$. The angles, θ_1 and θ_2 between two plates are 45° and −45°, respectively. The detailed procedure of numerical analysis for 2-D case is discussed in Appendix A.2.

When the excitation frequency is $f=5\,\text{kHz}$ and structural damping values of all plates are assumed to be $\eta=0.01$, hybrid power flow solutions can be obtained using the hybrid boundary condition of Eqs. (2.31)–(2.36) in all line junctions, as shown in Fig. 15. Though the coupling loss factor of SEA is used in

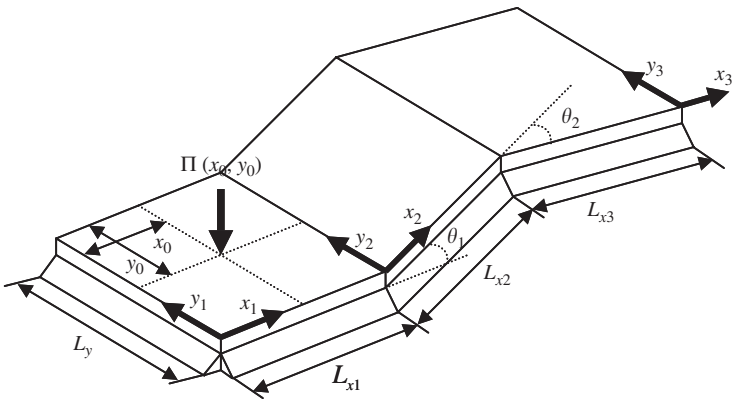

Fig. 14. Three finite plates jointed at arbitrary angles.

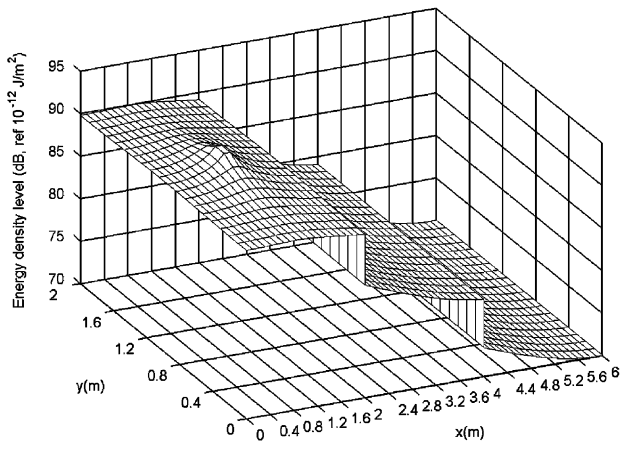

(a)

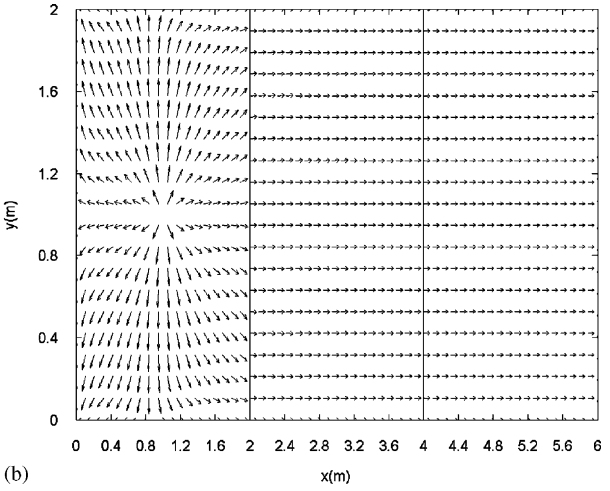

(b)

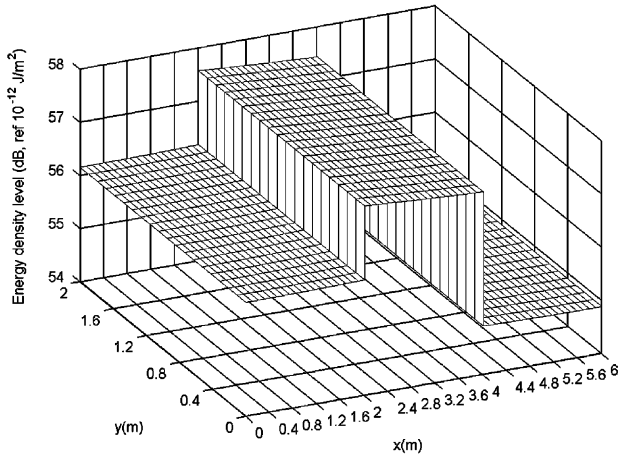

(c)

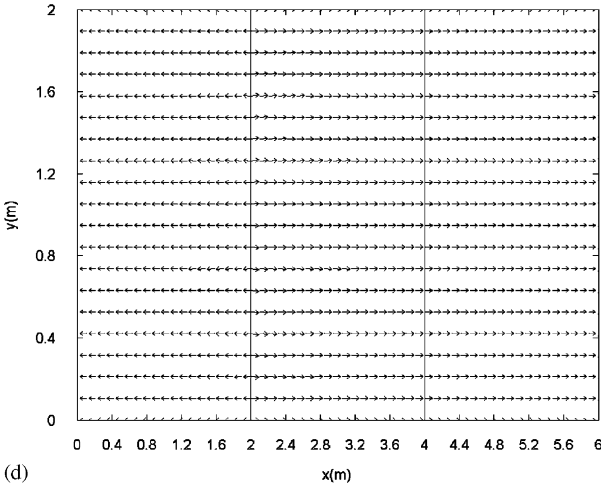

(d)

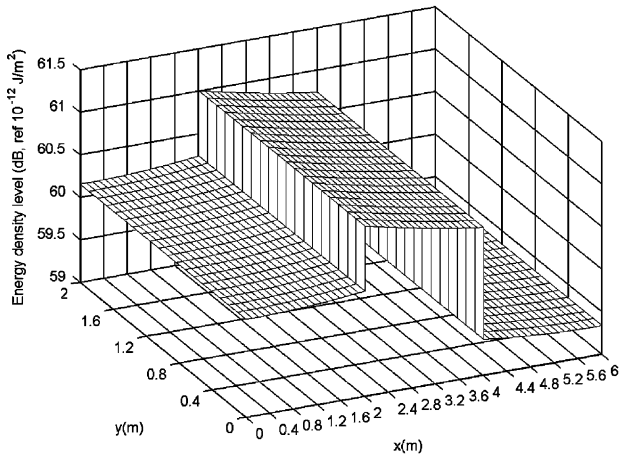

(e)

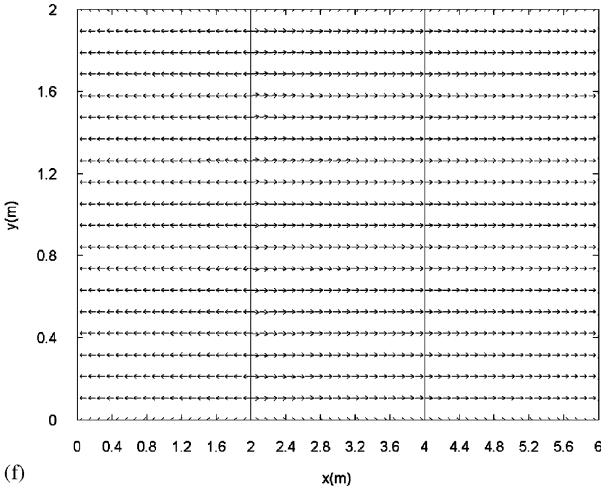

(f)

Fig. 15. Energy density and intensity distributions of hybrid power flow solution when $f = 5\,\text{kHz}$ and $\eta = 0.1$. (a) Flexural energy density; (b) flexural intensity; (c) longitudinal energy density; (d) longitudinal intensity; (e) shear energy density; (f) shear intensity.

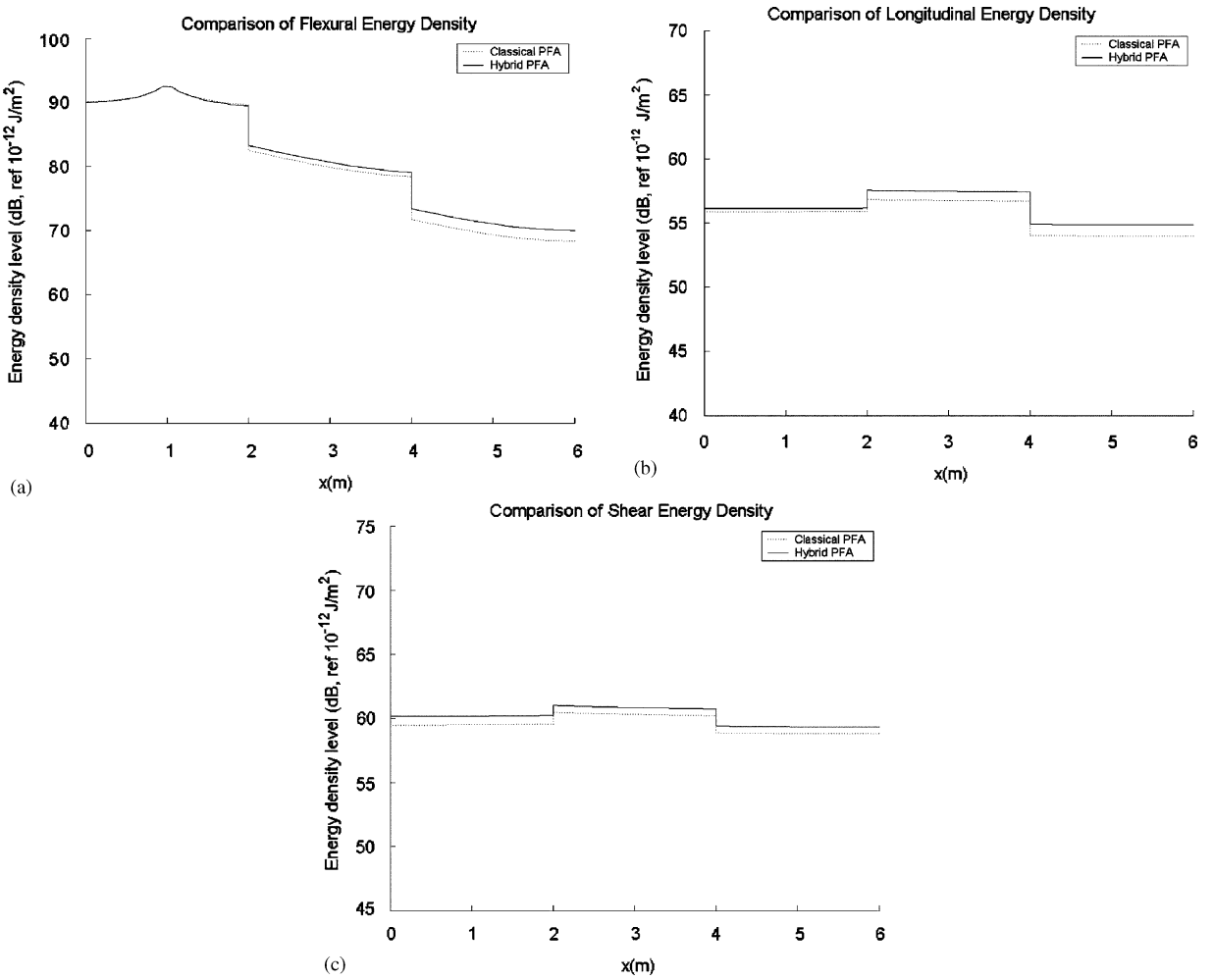

Fig. 16. The comparison of energy density using classical and hybrid boundary conditions in $y = L_y/2$ when $f = 5\,\text{kHz}$ and $\eta = 0.1$ ($\Re_f = 2.0017$, $\Re_l = 0.1636$, $\Re_s = 0.2826$): (a) flexural energy density; (b) longitudinal energy density; (c) shear energy density.

the boundary condition, the spatial variations of energy density and intensity are expressed well. Figs. 16 and 17 show the comparison of power flow solutions obtained using classical and hybrid boundary conditions when $\eta = 0.01$ and $\eta = 0.0001$, respectively. In Fig. 16, because the reverberance factors of all wave-fields in each subsystem are not small ($\Re_f = 2.0017$, $\Re_l = 0.1636$, $\Re_s = 0.2826$) due to high frequency and damping value, the difference between classical and hybrid power flow solutions is somewhat wide but is not more than 3 dB. However, because the reverberance factors of all wave-fields in each subsystem are very small ($\Re_f = 0.02$, $\Re_l = 0.0016$, $\Re_s = 0.0028$), hybrid power flow solution nearly agree with classical one in Fig. 17. Therefore, the hybrid boundary condition for power flow analysis is equivalent to the classical one in case of small reverberance factor. To definitely confirm these results, Figs. 18 and 19 show the effect of reverberance factors of wave-fields in each plate subsystem in the hybrid power flow solution. In Figs. 18 and 19, the hybrid power flow solution is compared with the classical power flow solution using each boundary condition at all joints. The results in these figures are the relative differences $(\|\overline{E_{3,\text{classic}}} - \overline{E_{3,\text{hybrid}}}\| / \|\overline{E_{3,\text{classic}}}\|)$ of space-averaged flexural (out-of-plane) and in-plane energy densities of plate 3, respectively, using classical and hybrid boundary conditions for various reverberance factors. Like the 1-D case, as the reverberance factors of each wave-field in plate subsystems become small, energy density levels obtained by two methods become equal.

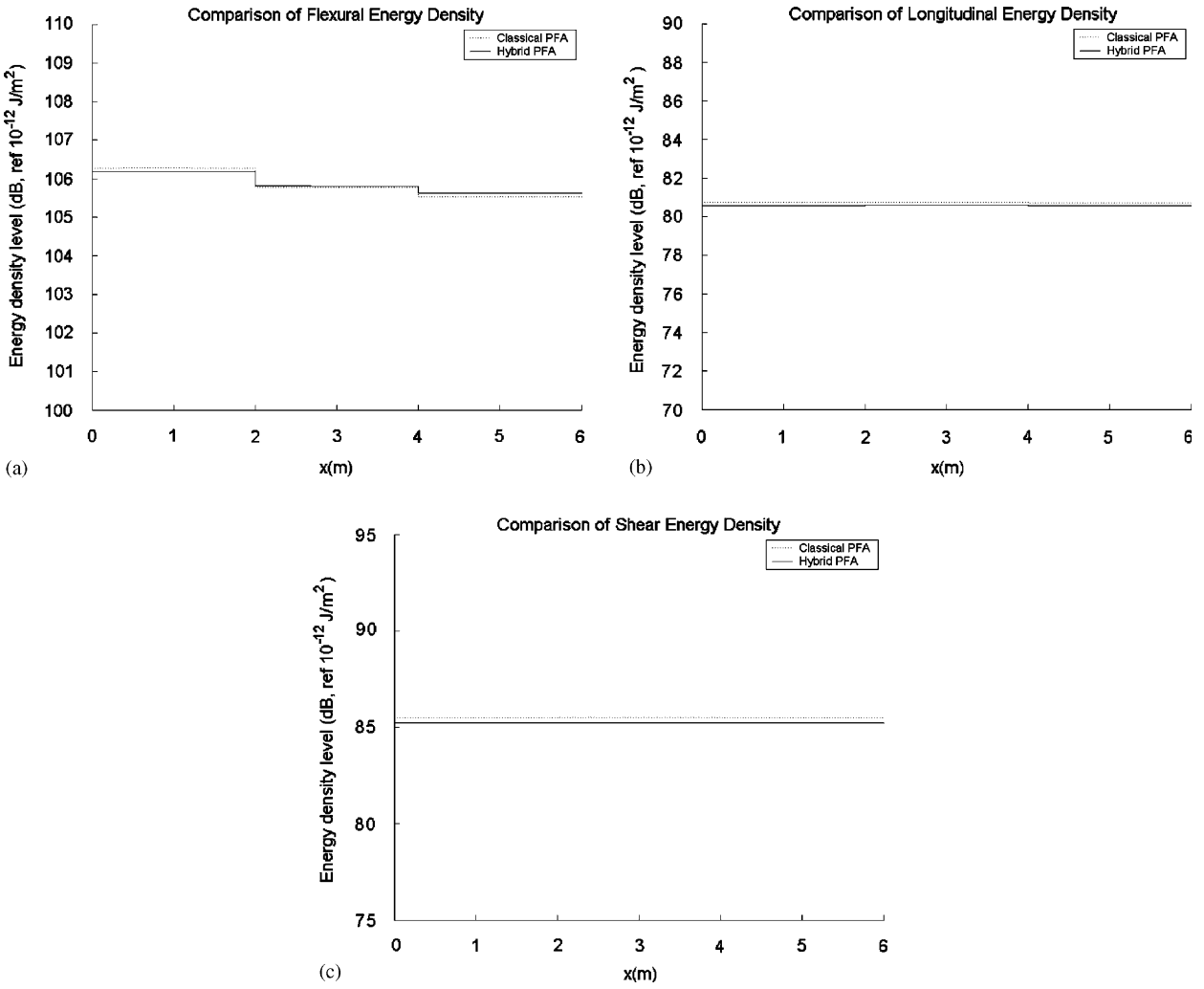

Fig. 17. The comparison of energy density using classical and hybrid boundary conditions in $y = L_y/2$ when $f = 5\,\text{kHz}$ and $\eta = 0.0001$ ($\Re_f = 0.02$, $\Re_l = 0.0016$, $\Re_s = 0.0028$): (a) flexural energy density; (b) longitudinal energy density; (c) shear energy density.

3. Conclusions

In this paper, the hybrid power flow analysis using SEA concepts was developed to effectively predict the vibrational and acoustic responses of low-damping structures and acoustic cavities in the medium-to-high frequency ranges. To develop the general hybrid method which uses the coupling relationship of SEA in power flow analysis, the hybrid boundary conditions including all kinds of wave-fields in one- and 2-D cases were derived, and numerical analyses for the validation of these boundary conditions were performed. Consequently, as the reverberance factor of the subsystem becomes small, the hybrid and classical power flow solutions become equal. Therefore, the developed hybrid power flow method can be a useful tool for the prediction of vibrational and acoustic responses, especially when it uses experimental coupling data for a low-damping system, if the hybrid boundary condition for 3-D case is derived and the hybrid PFFEM is developed to extend the application area of hybrid PFA to built-up structures, which are described in the other companion paper.

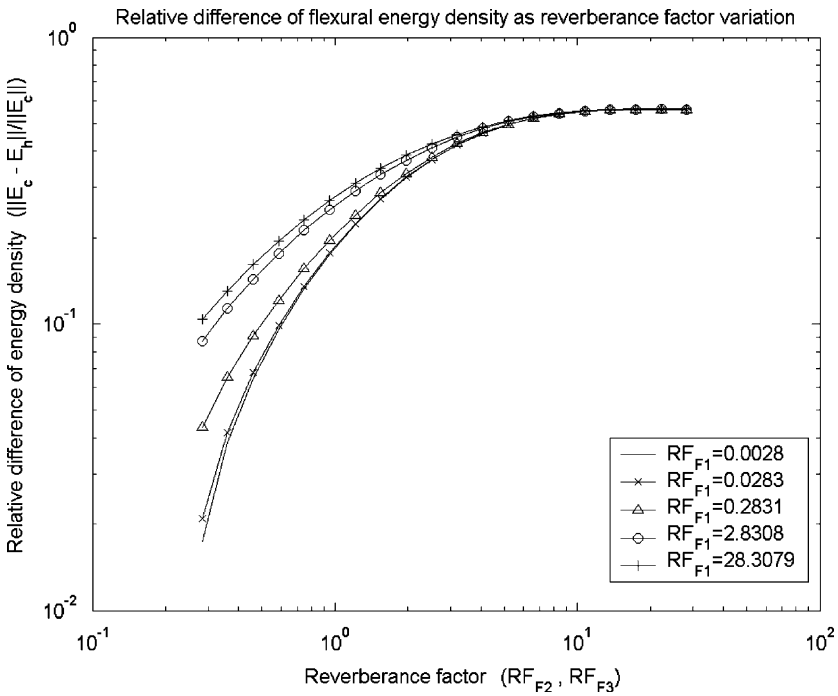

Fig. 18. Relative difference $\left(\|\overline{E_p}-\overline{E_h}\|/\|\overline{E_p}\|\right)$ of space-averaged flexural energy densities by two methods in plate 3 as the reverberance factor variations of plates 1 and 3. ——, $\Re_{f1}=0.0028$; —×—, $\Re_{f1}=0.0283$; —△—, $\Re_{f1}=0.2831$; —○—, $\Re_{f1}=2.8308$; —|—, $\Re_{f1}=28.3079$.

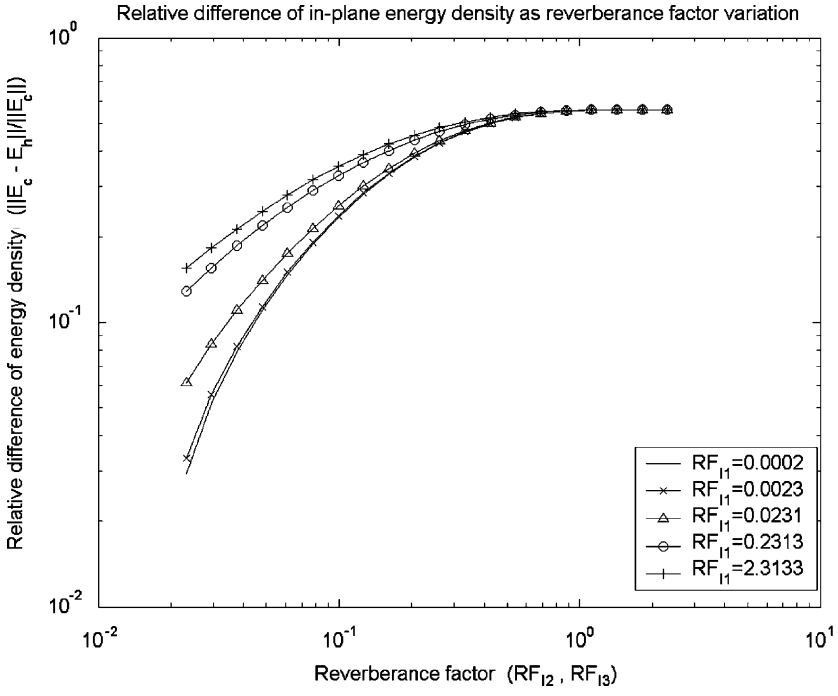

Fig. 19. Relative difference $\left(\|\overline{E_p}-\overline{E_h}\|/\|\overline{E_p}\|\right)$ of space-averaged in-plane energy densities by two methods in plate 3 as the reverberance factor variation of plates 1 and 3. ——, $\Re_{I1}=0.0002$; —×—, $\Re_{I1}=0.0023$; —△—, $\Re_{I1}=0.0231$; —○—, $\Re_{I1}=0.2313$; —|—, $\Re_{I1}=2.3133$.

Acknowledgements

This work was partially supported by Advanced Ship Engineering Research Center of the Korea Science and Engineering Foundation.

Appendix A

A.1. Numerical analysis of 1-D case

The equation and exact solution of flexural motion in beam i using Eq. (2.1) can be represented as, respectively,

$$E_{c,i}I_i\frac{\partial^4 w_i}{\partial x_i^4}+\rho_i S_i\frac{\partial^2 w_i}{\partial t^2}=F\delta(x_i-x_0)\,\mathrm{e}^{\mathrm{j}\omega t}, \tag{A.1}$$

and

$$w_i(x_i,t)=\left(A_i\mathrm{e}^{-\mathrm{j}k_{fi}x_i}+B\mathrm{e}^{\mathrm{j}k_{fi}x_i}+C\mathrm{e}^{-k_{fi}x_i}+D\mathrm{e}^{k_{fi}x_i}\right)\mathrm{e}^{\mathrm{j}\omega t}\quad(i=1,2,3,4), \tag{A.2}$$

where w_i is the transverse displacement of beam i and $k_{fi}=\left[\omega^2\rho_i S_i/E_{c,i}I_i\right]^{1/4}$ is the flexural wavenumber of beam i. The equation and exact solution of longitudinal motion in beam i can be expressed as, respectively,

$$E_{c,i}S_i\frac{\partial^2 u_i}{\partial x_i^2}-\rho_i S_i\frac{\partial^2 u_i}{\partial t^2}=-F_i\delta(x_i-x_0)\,\mathrm{e}^{\mathrm{j}\omega t}, \tag{A.3}$$

and

$$u_i(x_i,t)=\left(M_i\,\mathrm{e}^{-\mathrm{j}k_{li}x_i}+N_i\,\mathrm{e}^{\mathrm{j}k_{li}x_i}\right)\mathrm{e}^{\mathrm{j}\omega t}\quad(i=1,2,3), \tag{A.4}$$

where u_i is the longitudinal displacement of beam i and $k_{li}=\omega\left(\rho_i/E_{c,i}\right)^{1/2}$ is the longitudinal wavenumber of beam i. Because there are a total of 22 unknowns, the boundary conditions of the same number must be enforced.

The energy governing equations and power flow solutions for the m-type wave in beam p using Eqs. (2.10), (2.12) and (2.13) can be represented as, respectively,

$$-\frac{c_{g,mp}^2}{\eta_{mp}\omega}\frac{\mathrm{d}^2\langle e\rangle_{mp}}{\mathrm{d}x^2}+\eta_{mp}\omega\langle e\rangle_{mp}=\Pi_{\mathrm{in},mp}, \tag{A.5}$$

and

$$\langle e\rangle_{mp}=P_{mp}\,\mathrm{e}^{-\varphi_{mp}x_p}+Q_{mp}\,\mathrm{e}^{\varphi_{mp}x_p}, \tag{A.6}$$

where $\langle e\rangle_{mp}$, $c_{g,mp}$ and η_{mp} are the energy density, group velocity, and structural damping loss factor of m-type in beam p, respectively, and $\varphi_{mp}=\eta_{mp}\omega/c_{mp}$. In case of power flow solution, a total of 16 unknowns exist.

A.2. Numerical analysis of 2-D case

The energy governing equations for each wave in a thin plate given using Eq. (2.26) can be expressed as [8]

$$-\frac{c_{g,mj}^2}{\eta_{mj}\omega}\left(\frac{\mathrm{d}^2}{\mathrm{d}x_j^2}+\frac{\mathrm{d}^2}{\mathrm{d}y_j^2}\right)\langle e\rangle_{mj}+\eta_{mj}\omega\,\langle e\rangle_{mj}=\Pi_{\mathrm{in},mj},\quad(j=1,2,3,4\quad\text{and}\quad m=f,l,s), \tag{A.7}$$

where $\langle e\rangle_{mj}$, $c_{g,mj}$ and η_{mj} are the energy density, group velocity and structural damping loss factor of m-type in plate j, respectively. If the all y-directional boundary is simply supported like the model shown in Fig. 14, the analytic solution of Eq. (A.7) can be obtained as a single series solution,

$$\langle e\rangle_{mj}(x_j,y)=\sum_{n=0}^{\infty}E_{mj,n}\cos k_n y=\sum_{n=0}^{\infty}\left(A_{mj,n}^{+}\,\mathrm{e}^{-\lambda_{mj,n}x_j}+A_{mj,n}^{-}\,\mathrm{e}^{\lambda_{mj,n}x_j}\right)\cos k_n y, \tag{A.8}$$

where $E_{mj,n}$ is the nth component of the series solution, Eq. (A.8), $k_n = n\pi/L_y$ and $\lambda_{mj,n} = \sqrt{k_n^2 + (\eta_{mj}\omega/c_{g,mj})^2}$. The intensity of the m-type wave component in plate j can be obtained by the energy transfer relation, Eq. (2.27):

$$\langle q_x \rangle_{mj}(x_j, y) = \sum_{n=0}^{\infty} Q_{xmj,n} \cos k_n y = \sum_{n=0}^{\infty} \left\{ \left(\frac{c_{g,mj}^2}{\eta_{mj}\omega} \lambda_{mj,n} \right) \left(A_{mj,n}^{+} \mathrm{e}^{-\lambda_{mj,n} x_j} - A_{mj,n}^{-} \mathrm{e}^{\lambda_{mj,n} x_j} \right) \cos k_n y \right\}, \tag{A.9}$$

and

$$\left\langle q_y \right\rangle_{mj}(x_j, y) = \sum_{n=0}^{\infty} Q_{ymj,n} \sin k_n y = \sum_{n=0}^{\infty} \left\{ \left(\frac{c_{g,mj}^2}{\eta_{mj}\omega} k_n \right) \left(A_{mj,n}^{+} \mathrm{e}^{-\lambda_{mj,n} x_j} + A_{mj,n}^{-} \mathrm{e}^{\lambda_{mj,n} x_j} \right) \sin k_n y \right\}, \tag{A.10}$$

where $\langle q_x \rangle_{mj}$ and $\left\langle q_y \right\rangle_{mj}$ are the x- and y-components of intensity $\langle q \rangle_{mj}$.

In addition, the point input power can be approximated as

$$\Pi_m \delta(x - x_0)\delta(y - y_0) = \sum_{n=0}^{\infty} \Pi_{m,n}(x) \cos k_n y, \tag{A.11}$$

where Π_m is the input power of the m-type component. Here, $\Pi_{m,n}$, the nth component of Π_m can be expressed as

$$\Pi_{m,n} = \begin{cases} \dfrac{\Pi_m}{L_y}\delta(x - x_0) & (n = 0), \\ \dfrac{2\Pi_m}{L_y}\cos k_n y_0 \delta(x - x_0) & (n \neq 0). \end{cases} \tag{A.12}$$

The six unknowns in each plate's domain exist, and a total of 24 boundary conditions must be enforced. The power of each wave component is zero in the simply supported boundary and the continuity of energy density and power of each wave component in loading point must be enforced. In the line junction of a coupled plate, Eq. (2.40) is applied in classical power flow solutions, and Eqs. (2.37)–(2.39) are applied in hybrid power flow solutions.

References

[1] J.C. Wohlever, R.J. Bernhard, Mechanical energy flow models of rods and beams, *Journal of Sound and Vibration* 153 (1992) 1–19.

[2] O.H. Bouthier, R.J. Bernhard, Models of spaced-averaged energetics of plates, *AIAA Journal* 30 (3) (1992) 616–623.

[3] R.H. Lyon, R.G. DeJong, Theory and Application of Statistical Energy Analysis, Second ed., Butterworth-Heinemann, 1995.

[4] Y. Lase, M.N. Ichchou, L. Jezequel, Energy flow analysis of bars and beams: theoretical formulations, *Journal of Sound and Vibration* 192 (1) (1995) 281–305.

[5] R.S. Langley, On the vibrational conductivity approach to high frequency dynamics for two-dimensional structural components, *Journal of Sound and Vibration* 182 (1995) 637–657.

[6] Y.-H. Park, S.-Y. Hong, Hybrid power flow analysis using coupling loss factor of SEA for low-damping system—Part II: Formulation of 3-D case and hybrid PFFEM, *Journal of Sound and Vibration*, this issue, doi:10.1016/j.jsv.2006.03.056.

[7] H.G.D. Goyder, R.G. White, Vibrational power flow from machines into built-up structures: Part I, *Journal of Sound and Vibration* 68 (1980) 59–75.

[8] J.C.Wohlever, Vibrational Power Flow Analysis of Rods and Beams, Master of Science Thesis, Purdue University, 1988.

[9] D.-H. Park, S.-Y. Hong, H.-K. Kil, J.-J. Jeon, Power flow model and analysis of in-plane waves in finite coupled thin plates, *Journal of Sound and Vibration* 244 (2001) 651–668.